Journal of Engineering Science and Technology
9th EURECA 2017 Special Issue September (2018) 116 - 132

X-RAY DIFFRACTION ANALYSIS OF SCOMBEROMORUS GUTTATUS-DERIVED HYDROXYAPATITE AND MONTMORILLONITE ON POLYLACTIC ACID BIOCOMPOSITE

HON-MENG NG[1], SOO-TUEEN BEE[1,*], LEE TIN SIN[1], RATNAM, C. T.[2], A. R. RAHMAT[3]

[1]Department of Chemical Engineering, Lee Kong Chian Faculty of Engineering and Science, Universiti Tunku Abdul Rahman, Bandar Sungai Long, Jalan Sungai Long, 43000 Kajang, Selangor, Malaysia
[2] Radiation Processing Technology Division, Malaysian Nuclear Agency, Bangi, 43000 Kajang, Selangor, Malaysia
[3]Department of Polymer Engineering, Faculty of Chemical Engineering, Universiti Teknologi Malaysia, 81310 UTM Skudai, Johor, Malaysia
*Corresponding Author: direct.beest@gmail.com

Abstract

Up to date, the hydroxyapatite (HAp) as synthesized by chemical approaches has been widely investigated to provide reinforcement and bioactive sites for polylactic acid (PLA) as potential for application in bone grafting/regeneration field. However, the effect of HAp as derived from biogenic resources (e.g. fish bone) on polylactic acid has still not been well explored. Moreover, the further addition of HAp into PLA for better reinforcement is usually limited to low amount by its brittle ceramic nature. With an attempt to compensate for insufficient reinforcing effect of limited amount HAp on PLA, the addition of montmorillonite (MMT) as secondary reinforcing agent into PLA/HAp composite is thus proposed in this study. In order to prepare HAp for the synthesis of PLA/HAp/MMT composite, the collected fish bone waste of Mackerel fish (*Scomberomorus Guttatus* spp.) was mainly subjected to water boiling treatment and thermal calcination. The extracted HAp was then identified by several characterization techniques (FTIR, EDX, XRD, TGA) and melt blended with PLA and MMT at various composition using Brabender mixer. To evaluate the incorporation effect of biogenic HAp and MMT on fundamental properties of PLA biocomposites, the crystallographic structure of compounded PLA/HAp/MMT blends was investigated by XRD analysis. Results indicated the good effectiveness of HAp to promote PLA crystallization by the increased crystallinity of neat PLA. Meanwhile, this effect could be further enhanced after the addition of MMT by making the adjacent polymer chains to become closer. As calculated by using relevant XRD data, the increased value of *d*-spacing of MMT with an increase of HAp loading level also revealed the good ability of HAp to promote the intercalation of MMT into PLA matrix. Based on these findings, one can conclude that the fish bone waste derived-HAp and MMT could generate promising synergistic effect on improving the crystallographic structure of PLA.

Keywords: Biocomposites, Biomedical, Bone, Hydroxyapatite, Physical properties.

1. Introduction

Biodegradable polymer, poly (lactic acid) (PLA) which is derived from renewable resources found a favorable niche for application as bone fracture fixation materials in bone regeneration field mainly due to its biodegradation over time; therefore avoiding the second surgery for removal of an implant [1, 2]. The increasing role of PLA in the bone tissue engineering (BTE) also could be due to its degradation at a controlled rate, good processability and availability to produce in various shapes [3, 4]. However, the mechanical properties and thermal stability of PLA are often insufficient for load bearing and industrial applications in BTE [5, 6]. Note that the mechanical strength of biopolymer as candidate for load bearing bone implant should be high enough to match with those of human bone providing mechanical support during initial stage of bone formation [7, 8]. Meanwhile, the high thermal stability is necessary against the thermal degradation during industrial production since the toxic thermal decomposition product of PLA would be harmful to the living cells by trapping in polymer matrix [2, 7, 9]. Nevertheless, inorganic fillers in micro- and nanosizes such as hydroxyapatite (HAp) and nanoclay have been found to tackle above limitations through a small amount of addition, creating PLA composites with enhanced thermo-mechanical properties [2, 5, 10].

The incorporation of HAp ($Ca_{10}(PO_4)_6(OH)_2$) schematically presented in Fig. 1) can improve the mechanical and thermal properties of PLA composite via favorable organic-inorganic interaction between polymer-HAp to restrict polymer chains' mobility and the non-thermal degradable behaviour of HAp in the high temperatures range of 900-1200 °C [11-15]. As a major inorganic component of natural bone, the presence of HAp is also responsible for bone regeneration of composite implant by its promising bioactivity and osteoconductivity [1, 16]. It also makes directly bonds to the regenerated bones without mediatory tissues by the good bone binding ability [1, 17]. These behaviors could compensate for the lack of ability of pure PLA to induce osteogenesis or regeneration function of surrounding bone tissues due to its poor cellular attachment by the hydrophobic nature and absence of cell recognition sites [7, 17, 18]. More importantly, pH buffering effect of basic calcium phosphates ions released from the dissolution of HAp could neutralize the acidic molecules as decomposed from hydrolysis of PLA ester bonds that could induce unfavorable inflammatory response of the in-contact tissue and catalysis of the hydrolytic degradation [2, 9, 19-22]. However, it is common that the mechanical properties of prepared PLA/HAp composite are still lower than that of human bone unless the loading of a larger amount of HAp particles [23, 24].

In real application, however, it is considered impossible to load higher particles amount of HAp for PLA due to its high brittleness as would be aggravated by the increasing content of brittle ceramic filler (%elongation < 1 for HAp), which could result in improper plastic deformation that is necessary to withstand the stresses as imposed from patient's normal activity [25-27]. Thus, an additional reinforcement is necessary to assure the competitive mechanical properties of PLA-based bone graft implant, making the montmorillonite (MMT) to be proposed as the secondary enhancement element on PLA/HAp composite for present research work. As one of the most frequently studied nanoclay in PLA polymer systems, MMT is the most familiar species of smectide group, which consists of two fused tetrahedral silica thin layers sandwiching an edge-shared octahedral sheet of either magnesium or aluminum hydroxide [1, 3, 6, 28, 29]. The enhancement effect of MMT on mechanical and thermal properties of

organic polymer can be attributed to the nano-reinforcement effect of the intercalated/exfoliated layered silicates within polymer matrix and the high heat resistance of clay material [2, 6, 30, 31]. Moreover, the biocompatibility and safety of clays in medical application is widely supported in literature especially their same alkali nature with HAp that is important to neutralize the unfavorable acidic effect of PLA degradation product [3, 20, 32, 33].

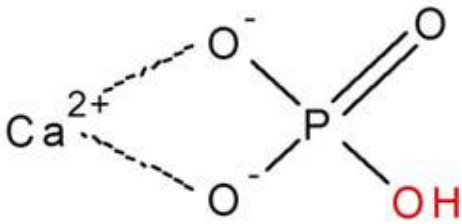

Fig. 1. Structural formula of hydroxyapatite.

Under above-mentioned backgrounds, the objective of present investigation is to develop new class of biodegradable material with much better performance, being potentially interesting for bone tissue engineering by adding HAp and MMT as secondary enhancement element into PLA composite. In order to achieve the established goal, it is of interest to study with as much detail as possible the synergistic effect of HAp and MMT on the structure and properties of PLA/HAp/MMT composite through characterizations on crystallographic structure by carrying out the XRD analysis. From the point of view of biomedical application, the present studied HAp filler is proposed to be derived from biogenic resources without involving any chemical precursors as traditionally used for in situ precipitation of HAp considering the health-risk problem of residual chemicals remaining on chemically-synthetic HAp [26, 34-36].

The other problems associated with chemical synthesis also include the high cost laborious process and difficulty to be scaled-up for industrial production [1, 13, 36-38]. More importantly, the reinforcing effect of biogenic HAp on PLA has still not been well explored to the best of our knowledge. Therefore, fish bone of Mackerel fish (*Scomberomorus Guttatus* spp.) was selected as biogenic resource to derive HAp, which is coded as MHAp for current research work. Meanwhile, the behind motivation of present research is also to convert fish bone waste into valuable product seeing the increasing disposal of fish bone from the food processing industry as waste currently that would cause serious environmental problem by the lack of appropriate waste management [39, 40].

As is well known, the easy occurrence of agglomeration of nanosize-filler (such as MMT) in polymer during melt processing was always to be questioned [41]. Thus, the loading level of present studied MMT was maximally bound to 4 phr by referring to the previous studies related to melt compounding of PLA/MMT composite as carried out by Shayan et al., 2015 [42] and Zaidi et al., 2009 [43] which found that the mechanical strength of PLA/MMT nanocomposites increased with an increase of MMT concentration up to 4 wt% but started to agglomerate at 5wt% that would cause the deterioration in properties of PLA composites.

2. Experimental

2.1. Materials

The polylactic acid pellets with injection grade of REVODE 101 (ρ = 1.31 g/cm^3 and MFI = 10-11 g/10 min) was purchased from Zhejiang Hisun Biomaterials Co., Ltd. This PLA was used as the base polymer in this study. The trimethylopropane trimethacrylate (TMPTMA) with industrial-grade containing 175 ppm monomethyl ether hydroquinone was supplied by Sigma-Aldrich (M) Sdn Bhd and was used as the cross-linking promoter in this study. The fish bone waste of Mackerel fish was collected from local restaurant and was used to derive MHAp as primary reinforcement in present study. The commercial grade of montmorillonite (MMT), Nanomer 1.3P was purchased from Nanocor, Arlington Height and was used as secondary reinforcement in PLA/HAp composite.

2.2. Preparation of Hydroxyapatite

The MHAp was obtained from fish bone waste of Mackerel fish after several crucible processes. Importantly, a fish bone without flesh or tissue remnants was necessary to be prepared first from the collected fish bone waste by subjecting to water boiling treatment for 4 hours. Next, the pretreated fish bone was continuously flushed with H_2O to ensure complete tissue removal followed by oven drying until constant weight is obtained. These dried fish bones then underwent thermal calcination process at 800°C for 4 hours in furnace. Afterwards, the calcined fish bones were crunched into HAp powder by using pestle and mortar. The successful extraction of MHAp was be confirmed by characterization techniques: Fourier transform infrared (FTIR) spectroscopy, scanning electron microscopy/energy dispersive X-ray spectroscopy (SEM/EDX), X-ray diffraction (XRD) test and Thermogravimetric analysis (TGA).

2.3. Preparation of Samples

PLA were compounded with MHAp, MMT and TMPTMA using a Brabender mixer at the heating temperature of 135 °C and rotor speed of 50 rpm for a mixing time of 8 min. The loading levels of PLA, MMT and TMPTMA were fixed at 100 phr, 0/2/4 phr and 3 phr, respectively while the loading levels of MHAp were varied from 2 to 10 phr.

2.4. X-ray Diffraction (XRD) Test

The compounded PLA/HAp/MMT blends were further characterized by XRD analysis by using a Shimadzu XRD 6000 diffractometer with CuKα radiation (λ = 1.542 Å) for a range of scattering angles 2θ ($3° < 2\theta < 40°$) at a scan rate of 2°/min. The test was performed at 30 kV and 30 mA with a thin-film attachment rotating at a speed of 50 rpm.

3. Results and Discussion

3.1. Characterizations of prepared MHAp

The HAp powder derived from fish bone waste of Mackerel fish (*Scomberomorus Guttatus* spp.) has been characterized by the FTIR, SEM/EDX, XRD and thermogravimetric analysis as shown in Figs. 2(a)-2(d).

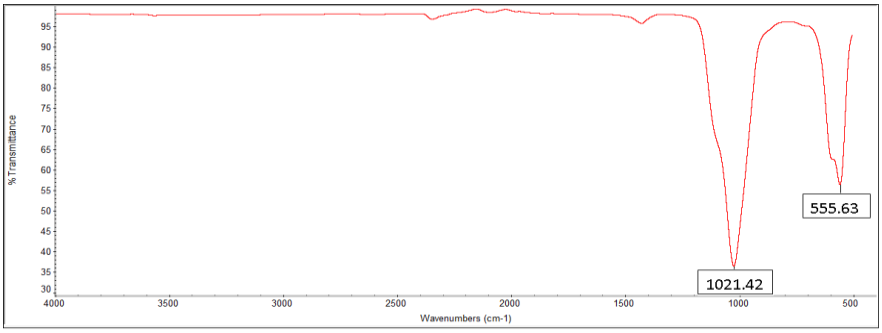

(a) FTIR spectrum

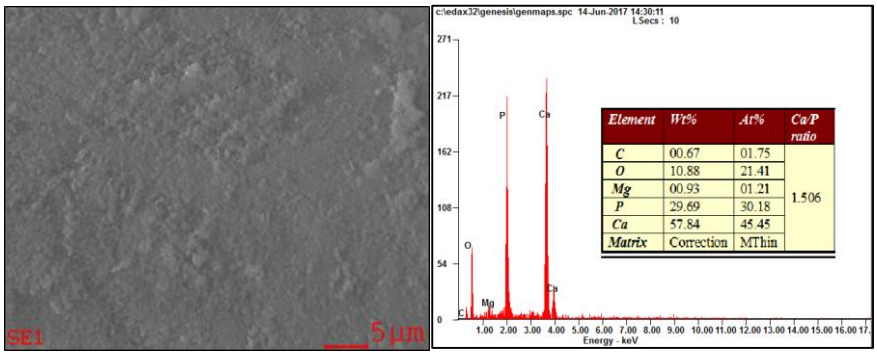

(b) SEM imaging with EDX (energy dispersive X-ray)

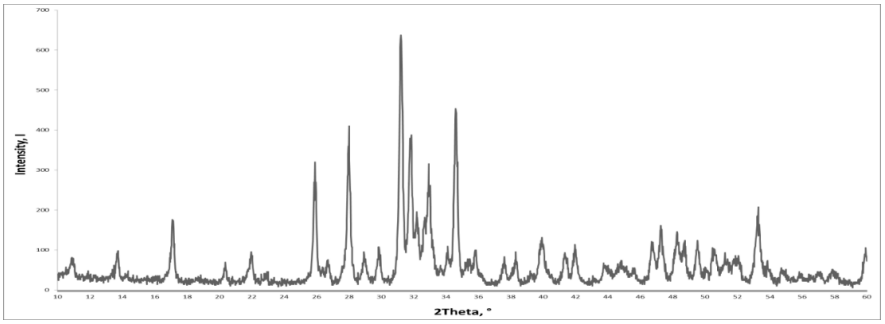

(c) XRD pattern

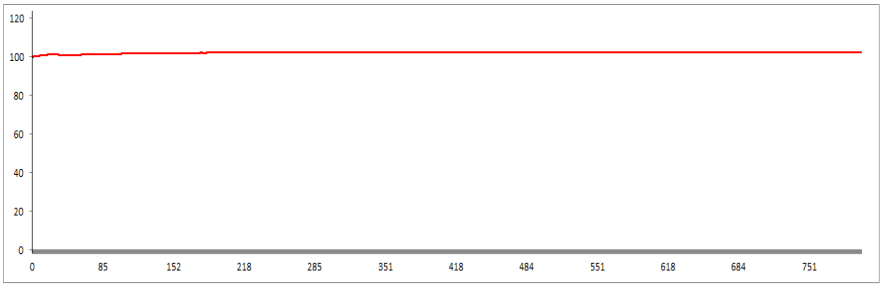

(d) TGA spectrum

Fig. 2. Characterization results of HAp extracted from fish bone waste of *Scomberomorus Guttatus* species.

The successful extraction of hydroxyapatite from Mackerel fish bone can be identified by chemical and elemental composition analysis of the MHAp samples using FTIR and EDX techniques, respectively. The presence of phosphate groups in MHAp can be evidenced by: (1) two prominent absorption peaks located at 1021.42 cm^{-1} and 555.63 cm^{-1}, Fig. 2(a), corresponding to the stretching modes and the bending modes (O-P-O bonds) of PO_4^{3-} vibration, respectively [1, 16, 44], (2) the presence of phosphorus and oxygen peak in EDX spectrum, Fig. 2(b). Another main element, calcium, which constitutes the HAp also has been proved by the presence of Ca peak in EDX. Moreover, the XRD pattern of MHAp also showed the presence of the major HAp peaks at 27.975°, 31.201°, 34.592° 2θ angles as shown in Fig. 2(c). Meanwhile, the appearance of strongest XRD peak at 31.201° also matches with the strongest HAp peak in the 2theta range of 31°~32° for a standard hydroxyapatite as reported elsewhere [11].

It is also important to examine whether the secondary phases (Tricalcium phosphate, CaO etc.) and organic impurities occurred or not in the HAp after being extracted by calcination, however, their absence can be verified by: (1) lower Ca/P ratio in MHAp than in HAp associated with CaO, (2) no evolution of peaks corresponding to Tricalcium phosphate (TCP) was observed from the XRD analysis, (3) absence of mass loss in TGA graph, Fig. 2(d) or any characteristic band (e.g C-H bonding) in FTIR spectrum corresponding to organic matter. For the statement (1), the Ca/P ratio of MHAp was calculated as 1.506 from EDX analysis, which is indicative of the absence of CaO as secondary phase since the EDX result would give to higher Ca/P ratio (~2.13) for the HAp attached by CaO phase [45]. Such CaO phase is usually decomposed from the calcinations (beyond 650 °C) of fish bone according to the decomposition reaction of HAp: $Ca_{10}(PO_4)_6(OH)_2$----->$Ca_3(PO_4)_2$ + CaO + H_2O, where $Ca_3(PO_4)_2$ is referred to tricalcium phosphate (TCP) [11, 46].

Implicitly, TCP phase also would not be liberated as secondary phase in MHAp under the absence of CaO phase, which is in agreement with the beforementioned statement (2). Without the presence of any secondary phases and organic impurities, the as-prepared MHAp is thus in form having high phase purity [13, 17, 47], meaning that the good interfacial interaction between MHAp and PLA matrix can be expected. The absence of secondary phase also represents the formation of stoichiometric structure of HAp [46], however the obtained Ca/P ratio (1.506) is slightly lower than but close to the stoichiometric value of 1.67, and hence nearly stoichiometric MHAp was successfully produced with this sample. A little of discrepancy is attributed to the disturbance from trace amounts of substituting ions such as cations (Mg^{2+}) as indicated in EDX spectrum that would affect the Ca/P ratio of HAp [13, 37]. Favorably, presence of Mg ions is additional advantage as Mg is a vital element required for enhancement in bone regeneration process [7, 13]. Meanwhile, since there is lack of any secondary phase or organic impurities as additional components in nearly stoichiometric MHAp, its consequently excellent compositional homogeneity can be used to stabilize it against decomposition at elevated temperatures, contributing to higher thermal stability during composite processing [11].

For HAp being hydrophilic in nature, It is supposed that -OH stretching and vibrational band exist at around 3500-3700 cm^{-1} as broad peak and 600-650 cm^{-1} respectively in the FTIR spectrum of lamellar MHAp, however, they cannot be observed because of their low severity in HAp [48]. The poor hydrophilicity of

MHAp as resulted from its lack of surface hydroxyl groups can be further proved by: (1) the absence of a broad peak in the range of 3000-3600 cm^{-1} as assigned to adsorbed H_2O in the HAp powder [16, 48], (2) the absence of initial mass loss (at temperature around 100°C) related to the removal of adsorbed water molecules as indicated in TGA graph [21, 49].

It is believed that the OH groups have been mostly displaced by carbonate (CO_3^{2-}) ions, resulting in the formation A-type carbonated apatite as typically occurred in biological system [13, 50]. This can be further supported by several evidences from: (1) FTIR spectrum which exhibits a very weak $\nu_3CO_3^{2-}$ band at around 1450-1500 cm^{-1} [10, 21, 44], (2) the presence of carbon peak in EDX spectrum that should not be belonged to the organic impurities. Moreover, the presence of carbonate (CO_3^{2-}) ions also can be used to explain the lower Ca/P ratio in MHAp. Beneficially, the lower occurrence of HAp filler agglomeration in composite can be expected in the present study by the decreased surface charge energy on MHAp as the amount of surface OH- groups have been reduced by the A-type carbonate ions substitution. Moreover, the carbonated apatite is closely related to the mineral component of human bone, it is advantageous for enhancement in osteoconductivity contributing to aid bone formation during implantation [50].

3.2. XRD study of prepared composite samples

The X-ray diffraction analysis is usually conducted to evaluate the crystallography structure, dispersion state of filler and degree of crystallinity of polymer matrix. The XRD patterns of pristine PLA and PLA composite filled with various content of MHAp and MMT are shown in Figs. 3(a)-3(c). The XRD patterns are characterized in the 2θ range of 3°-40°. All related XRD data are summarized in Table 1. The degree of crystallinity (%Xc) was calculated as the percentage of the scattered intensity of the crystalline phase over the scattered intensity of the crystalline and amorphous phase. Based on the obtained angle and FWHM of the diffraction peak, the crystallite size (L) and d-spacing (d) can be calculated using the Scherrer and Bragg's formula respectively, which are given in Eqs. (1) and (2):

$$L = \frac{k\lambda}{\beta cos\theta} \tag{1}$$

$$d = \frac{\lambda}{2sin\theta} \tag{2}$$

where λ = 1.542 Å is the wavelength of the Cu-Kα X-ray radiation used, B (in radians) is the full width at half maximum (FWHM) of the diffraction peak, θ is the Bragg angle (in radians), k is the Scherrer constant (taken to be 0.9).

The XRD patterns of all PLA composites added with increasing of loading level of MHAp are shown in Fig. 3(a). Accordingly, five significant diffraction peaks occur at 2θ range of 13.5°-13.6° (Peak A), 16.3°-16.4° (Peak B), 17.8°-17.9° (Peak C), 24.9°-25.0° (Peak D), 37.8°-37.9° (Peak E). However, these five diffraction peaks were absent on XRD curve of neat PLA instead of replacing the original PLA diffraction peak as located at 22.91°, 29.64°, 36.21°, 39.64°, bringing about higher crystallinity (~35-39%) than that of pristine PLA (14.38 %) as shown in Table 1.

This implies that the dispersed MHAp particle has fully ruptured the highly ordered chain arrangement structure in crystallite of original PLA peaks into random chain arrangement structure during melt processing and facilitated the recrystallization process throughout the PLA amorphous phase for new crystal structural arrangement at numerous locations. Thus, one can conclude that the MHAp fillers have high tendency to act as heterogeneous nucleating agents effective for promoting the crystallization for PLA by providing preferential nucleation sites, thus favoring a higher %Xc of composite as compared to that of unfilled PLA [9, 51]. By the existence of nucleating agent in free space between polymer chains in amorphous phase, the minimization of free space between polymer chains could be achieved under the presence of interfacial interaction between HAp-polymer [25, 48]. Indeed, a good interfacial interaction is essential for the nucleating agent (HAp) driving the adjacent polymer chains to initiate the nucleation of crystallites during polymer crystallization process [48, 52].

In general, the formation of favorable inorganic-organic interaction between HAp and PLA in form of chemical bonding can be achieved via: (1) the hydrogen bonding between oxygen atom of PO_4^{3-} and hydrogen atom of polymer COOH group [53], (2) the hydrogen bonding between the =O sites of polymer carbonyl groups and -OH group of HAp [1, 10, 11] and (3) chemical linkage between oxygen atom in the ester group double bond of PLA and Ca^{2+} in the HAp in form of weak ionic bond namely chelation [24, 53]. However, the organic-inorganic interaction as stated in case (2) can be excluded from the present study since there is lack of -OH groups in MHAp as discussed before. But the lack of surface -OH groups is contributable to avoid the occurrence of HAp filler aggregation by the lower particle surface energy and thus ensure the good interfacial interaction between MHAp-PLA even at higher loading level. This can be proved by the fact that PLA composites filled with 6/8/10 phr of MHAp still keep high crystallinity even their peak intensity and crystallite size for peak A, B and C is significantly decreased following after the incorporation of 4 phr MHAp, which is mainly compensated by the appearance of extra peak E (formation of relatively large size crystallite) that is absent for composites filled with 2 and 4 phr MHAp.

Regarding to the calculated d-spacing as tabulated in Table 1, the increasing of MHAp portion from 2 phr to 10 phr did not exhibit a significant effect on d-spacing of all diffraction peaks (peaks A, B, C, D and E). This implies that the close packing of polymeric macromolecular chains arrangement happens in all developed crystalline regions (crystallites), while the same reason as that for the PLA composites filled with 2 or 4 phr MMT could be applied. This shows that the addition of either MHAp and/or MMT particles did not affect the compactness of macromolecular chain in all the crystalline regions.

After the addition of 2 phr MMT in PLA/MHAp composite, the peak intensity of A, B, C and D is significantly increased with respect to that of all composite without MMT, which is also accompanied by the appearance of extra peak E, Fig. 3(b) for composite filled with 2/4 phr MHAp that is absent in Fig. 3(a). This can be due to the successful intercalation of MMT into PLA matrix as proved by the enhanced d-spacing of silicate layer (relative to its original spacing) according to Table 2, subsequently making the adjacent polymer chains to become closer.

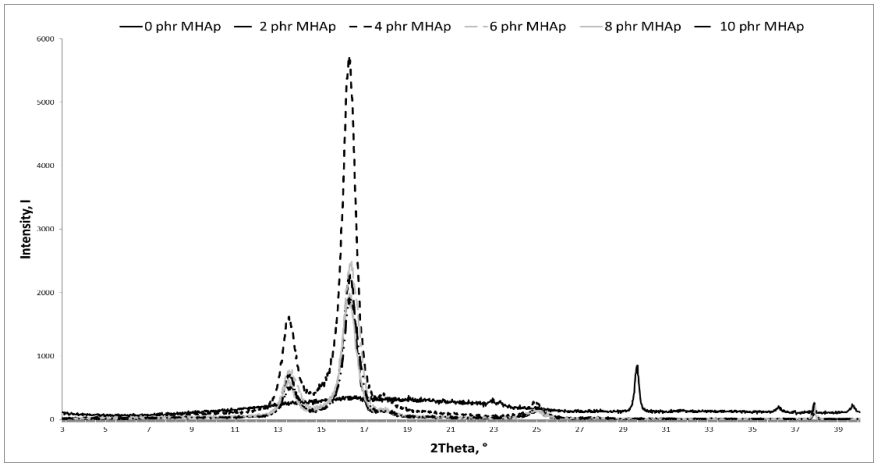

(a) 0 phr MMT

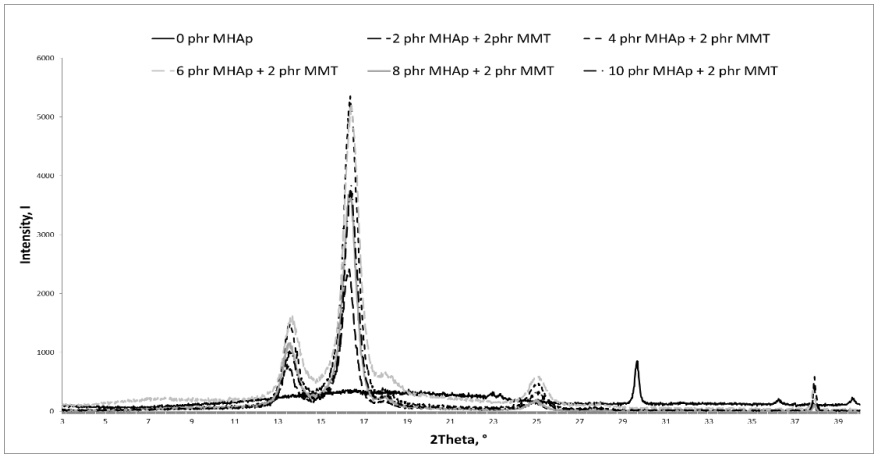

(b) 2 phr MMT

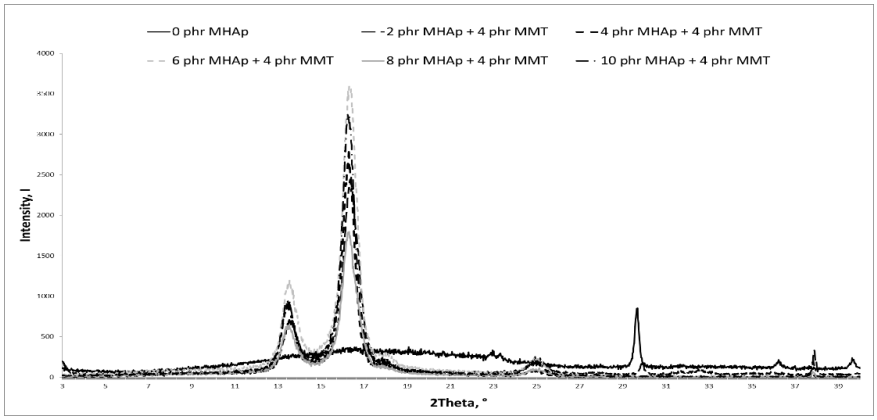

(c) 4 phr MMT

Fig. 3. XRD pattern curves for PLA/MHAp compositesadded with various loading level of MMT under increasing of MHAp loading level from 0 phr to 10 phr.

Therefore, the minimization of the free space between polymer chains by the presence of MHAp could be further decreased by MMT, enabling surrounding polymer chains to crystallizing more in a higher efficiency under the nucleation effect of MHAp. Moreover, Table 2 also presents the inter-chain separation (*R*) for MMT and MMT added PLA/MHAp composite which was determined from Klug and Alexander equation as shown in Eq. (3):

$$R = \frac{5\lambda}{8sin\theta} \tag{3}$$

It is found that the *d*, change of d-spacing (Δd) and *R* of MMT in polymer matrix is enhanced by an increasing MHAp content from 2/4 phr to 8 phr, indicating the improved dispersion and intercalation state of MMT by the presence of MHAp. The possible explanation could be the high tendency of repulsive interaction occurred between PO_4^{3-} groups of MHAp and the negative sites in MMT clay structure [54, 55] to facilitate the melt intercalation of PLA into the MMT galleries during melt blending under homogeneous distribution of MHAp. As certain amount of PLA chains are introduced into the MMT galleries, the available free space to the polymer chains is thus decreased by MHAp in an easier way, contributing to facilitate the crystal structural arrangement consequently. This can be verified by the increased crystallite size for major deflection peaks of PLA/MHAp composite, development of small crystalline region (as peak E) and the increased %Xc of PLA composite filled with 4/6 phr MHAp after the addition of 2 phr MMT, as referred to Table 2.

As compared to Fig. 3(b), the increasing addition of MMT from 2 to 4 phr has decreased the peak intensity of major diffraction peaks of PLA/MHAp composite especially filled with 4/6/8 phr MHAp. This fact can be further supported by the reduction in %Xc or crystallite size of mostly all of 2 phr MMT added composites and disappearance of peak E of 2 phr MMT added composites filled with 4/6/8 phr MHAp after further addition of MMT content up to 4 phr. The possible explanation is the existence of higher degree of intercalated structure for MMT as indicated by the larger value of *d*, change of d-spacing (Δd) and *R* of silicate layer (referred to Table 2), enabling the more extensive PLA chains to be intercalated into clay galleries [55]. Such a higher degree of intercalated structure for 4 phr MMT might be due to the more prominent occurence of repulsive interaction between MMT and MHAp at higher MMT loading level during compounding, which further facilitating the intercalation of MMT into PLA matrix.

By the restriction effect of large surface area silicate layer on the extensive intercalated polymer chains, the movement of surrounding polymer chains (amorphous phase) is inhibited for folding and arranging crystallization under nucleating effect of MHAp [6]. In other words, as more polymer chains introduced into MMT gallaries, less polymer chains participate in PLA crystallization as promoted by MHAp, explaining the reduced peak intensities, %Xc and crystallite size of PLA/MHAp composite when added with higher MMT loading level. However, even the peak densities of major diffraction peaks decreased by the addition of MMT from 2 to 4 phr, almost peak intensities and crystallite siz still keep higher than that of composities without MMT especially when filled with 4/10 phr MHAp, indicating the promising synergistic effect of MHAp and MMT on improving the crystallographic structure of PLA.

Table 1. The 2θ, crystallite size (L) and d-spacing for deflection peaks A, B, C, D and E on XRD pattern curves (in Fig. 3(a)-(c) of PLA composites added with various loading levels of MHAp and MMT.

Loading level, phr (MHAp/MMT)	Deflection peak A			Deflection peak B			Deflection peak C			Deflection peak D			Deflection peak E			%Xc
	2θ,°	L, Å	d,Å	2θ,°	L, Å	d,Å	2θ,°	L, Å	d,Å	2θ,°	L, Å	D,Å	2θ,°	L, Å	d,Å	
0/0	Nil	Nil	Nil	Nil	Nil	Nil	Nil	Nil	Nil	Nil	Nil	Nil	Nil	Nil	Nil	14.38
2/0	13.519	125.94	6.54	16.316	124.48	5.43	17.840	99.24	4.97	24.973	116.61	3.56	Nil	Nil	Nil	39.49
4/0	13.514	113.07	6.54	16.286	119.85	5.44	17.860	94.62	4.96	24.892	119.19	3.57	Nil	Nil	Nil	35.38
6/0	13.592	99.21	6.51	16.393	102.41	5.40	Nil	Nil	Nil	25.057	97.54	3.55	37.868	207.43	2.37	35.10
8/0	13.487	120.00	6.56	16.292	114.01	5.43	17.820	80.71	4.97	24.890	110.19	3.57	37.801	213.37	2.38	36.87
10/0	13.607	100.65	6.50	16.391	106.40	5.40	17.940	85.89	4.94	25.021	106.24	3.55	37.858	205.19	2.37	37.27
2/2	13.466	120.36	6.57	16.249	123.02	5.45	17.700	72.02	5.00	24.882	121.56	3.57	37.800	228.98	2.38	35.59
4/2	13.570	110.93	6.52	16.357	113.66	5.41	17.940	92.41	4.94	24.998	110.41	3.56	37.875	213.81	2.37	36.77
6/2	13.656	94.99	6.48	16.398	102.80	5.40	18.000	67.94	4.92	25.027	101.04	3.55	37.793	200.26	2.38	36.68
8/2	13.540	110.42	6.53	16.316	117.49	5.43	17.920	104.67	4.94	24.912	112.49	3.57	Nil	Nil	Nil	36.28
10/2	13.570	116.86	6.52	16.370	119.05	5.41	17.920	88.62	4.94	25.010	112.83	3.56	37.870	223.06	2.37	37.03
2/4	13.594	101.58	6.51	16.384	104.46	5.40	17.900	83.75	4.95	25.021	99.51	3.55	37.857	198.34	2.37	31.92
4/4	13.469	121.36	6.57	16.256	128.10	5.45	17.820	97.08	4.97	Nil	Nil	Nil	Nil	Nil	Nil	36.86
6/4	13.546	107.03	6.53	16.321	110.03	5.42	17.920	89.33	4.94	24.948	98.76	3.56	Nil	Nil	Nil	32.19
8/4	13.517	104.94	6.54	16.306	103.86	5.43	18.200	144.13	4.87	25.017	86.35	3.56	Nil	Nil	Nil	30.70
10/4	13.470	118.83	6.56	16.270	122.25	5.44	17.760	82.69	4.99	24.900	113.52	3.57	37.810	234.33	2.38	35.19

Remarks: Nil = No peak detected

Table 2. The angle, *d*-spacing, change of *d*-spacing and inter-chain separation of 2 and 4 phr MMT added PLA composites filled with increasing of amount MHAp.

Loading level, phr (MHAp/MMT)	2θ,°	*d*, Å	Δd, Å	*R*, Å
MMT	1.049	84.13	-	105.16
2/2	0.827	106.73	22.60	133.42
4/2	0.847	104.19	20.06	130.23
8/2	0.788	111.95	27.82	139.93
2/4	0.746	118.28	34.15	147.85
4/4	0.749	117.88	33.75	147.35
8/4	0.740	119.24	35.11	149.05

Notes: these data were obtained upon XRD analysis in the 2θ range from 0° to 3°.

4. Conclusions

Overall, the hydroxyapatite in form of A-type-carbonated-apatite without any secondary phase or organic impurities has been successfully extracted from fish bone waste of Mackerel fish, as verified by the characterization techniques of FTIR, EDX, XRD and TGA.

With high phase purity of extracted MHAp surface, it could effectively interact with PLA by favorable organic-inorganic interaction between their functional groups, hence effectively driving the adjacent polymer chains to initiate nucleation of PLA crystallites and even recrystallization throughout amorphous phase based on XRD analysis.

Such nucleating effect of MHAp on improving crystallinity of PLA by minimizing the free space between polymer chains can be further enhanced under the presence of MMT which could improve the efficiency of nucleation of crystallites during crystallization process by the melt intercalation of PLA into clay galleries.

The good intercalation state of MMT in PLA matrix has been confirmed by the higher interlayer spacing than that of pure MMT and also could be further improved by the increasing of MHAp loading level due to the high tendency of repulsive interaction between phosphate groups of MHAp and the negative sites in MMT to facilitate the delamination of MMT in PLA matrix.

Eventhough there would be more extensive PLA chains to be intercalated into clay galleries at higher MMT loading level by the more prominent occurrence of repulsive interaction between MMT and MHAp, however, this also implied that more polymer chains would be inhibited in movement for participating in the PLA crystallization process as promoted by the nucleating effect of MHAp.

Therefore, further increment in MMT loading level from 2 phr to 4 phr has caused the reduction in crystallinity and crystallinite size of PLA matrix.

Nomenclatures

d	Interplanar distance (d-spacing), Å
k	Scherrer constant, 0.9
L	Crystallite size, Å
R	Inter-chain separation, Å

Greek Symbols

β	Diffraction peak width, radian
λ	X-ray wavelength, 1.542 Å
θ	Angle between the beam and the normal to the reflecting plane, radian
ρ	Density, g/cm^3

Abbreviations

MHAp	Mackerel-derived Hydroxyapatite
MMT	Montmorillonite
PLA	Poly (lactic acid)
phr	parts per hundred (polymer resin)
XRD	X-ray diffraction

References

1. Wan, Y.Z.; Wu, C.Q.; Xiong, G.Y.; Zuo, G.F.; Jin, J.; Ren, K.J.; Zhu, Y.; Wang, Z.R.; and Luo, H.L. (2015). Mechanical properties and cytotoxicity of nanoplate-like hydroxyapatite/polylactide nanocomposites prepared by intercalation technique. *Journal of the Mechanical Behavior of Biomedical Materials*, 47, 29-37.
2. Castro-Aguirre, E.; Iñiguez-Franco, F.; Samsudin, H.; Fang, X.; and Auras, R. (2016). Poly(lactic acid)—Mass production, processing, industrial applications, and end of life. *Advanced Drug Delivery Reviews*, 107, 333-366.
3. Nieddu, E.; Mazzucco, L.; Gentile, P.; Benko, T.; Balbo, V.; Mandrile, R.; and Ciardelli, G. (2009). Preparation and biodegradation of clay composites of PLA. *Reactive and Functional Polymers*, 69(6), 371-379.
4. Malwela, T.; and Ray, S.S. (2015). Enzymatic degradation behavior of nanoclay reinforced biodegradable PLA/PBSA blend composites. *International Journal of Biological Macromolecules*, 77, 131-142.
5. Fukushima, K.; Tabuani, D.; Arena, M.; Gennari, M.; and Camino, G. (2013). Effect of clay type and loading on thermal, mechanical properties and biodegradation of poly(lactic acid) nanocomposites. *Reactive and Functional Polymers*, 73(3), 540-549.
6. Sermsantiwanit, K.; and Phattanarudee, S. (2012). Preparation of bio-based nanocomposite emulsions: Effect of clay type. *Progress in Organic Coatings*, 74(4), 660-666.
7. Lijuan, X.; Liuyun, J.; Chengdong, X.; Lixin, J.; and Ye, L. (2014). Study on a novel double-layered composite membrane of Mg-substituted nano-hydroxyapatite/poly(L-lactide-co-ε-caprolactone): Effect of different L-lactide/ε-caprolactone ratios. *Materials Science and Engineering: A*, 615, 361-366.

8. Hong, Z.; Zhang, P.B.; He, C.L.; Qiu, X.Y.; Liu, A.X.; Chen, L.; Chen, X.S.; and Jing, X.B. (2005). Nano-composite of poly(L-lactide) and surface grafted hydroxyapatite: Mechanical properties and biocompatibility. *Biomaterials*, 26(32), 6296-6304.
9. Mathieu, L.M.; Bourban, P.E.; and Ma˚nson, J.A.E. (2006). Processing of homogeneous ceramic/polymer blends for bioresorbable composites. *Composites Science and Technology*, 66(11-12), 1606-1614.
10. Dadbin, S.; and Kheirkhah, Y. (2014). Gamma irradiation of melt processed biomedical PDLLA/HAP nanocomposites. *Radiation Physics and Chemistry*, 97, 270-274.
11. Choi, D.; Marra, K.G.; and Kumta, P.N. (2004). Chemical synthesis of hydroxyapatite/poly(ε-caprolactone) composites. *Materials Research Bulletin*, 39(3), 417-432.
12. Yuan, Q.H.; Qin, C.P.; Wu, J.B.; Xu, A.P.; Zhang, Z.Q.; Liao, J.Q.; Lin, S.X.; Ren, X.Z.; and Zhang, P.X. (2016). Synthesis and characterization of Cerium-doped hydroxyapatite/polylactic acid composite coatings on metal substrates. *Materials Chemistry and Physics*, 182, 365-371.
13. Akram, M.; Ahmed, R.; Shakir, I.; Ibrahim, W.A.W.; and Hussain, R. (2013). Extracting hydroxyapatite and its precursors from natural resources. *Journal of Materials Science*, 49(4), 1461-1475.
14. Li, J.; Zheng, W.; Li, L.; Zheng, Y.F.; and Lou, X. (2009). Thermal degradation kinetics of g-HA/PLA composite. *Thermochimica Acta*, 493(1-2), 90-95.
15. Chung, E.J.; Sugimoto, M.J.; and Ameer, G.A. (2011). The role of hydroxyapatite in citric acid-based nanocomposites: Surface characteristics, degradation, and osteogenicity in vitro. *Acta Biomaterialia*, 7(11), 4057-4063.
16. Nga, N.K.; Giang, L.T.; Huy, T.Q.; Viet, P.H.; and Migliaresi, C. (2014). Surfactant-assisted size control of hydroxyapatite nanorods for bone tissue engineering. *Colloids and Surfaces B: Biointerfaces*, 116, 666-673.
17. Torabinejad, B.; Mohammadi-Rovshandeh, J.; Davachi, S.M.; and Zamanian, A. (2014). Synthesis and characterization of nanocomposite scaffolds based on triblock copolymer of L-lactide, ε-caprolactone and nano-hydroxyapatite for bone tissue engineering. *Materials Science and Engineering: C*, 42, 199-210.
18. Chlopek, J.; Rosol, P.; and Morawska-Chochol, A. (2006). Durability of polymer-ceramics composite implants determined in creep tests. *Composites Science and Technology*, 66(11-12), 1615-1622.
19. Simpson, R.L.; Nazhat, S.N.; Blaker, J.J.; Bismarck, A.; Hill, R.; Boccaccini, A.R.; Hansen, U.N.; and Amis, A.A. (2015). A comparative study of the effects of different bioactive fillers in PLGA matrix composites and their suitability as bone substitute materials: A thermo-mechanical and in vitro investigation. *Journal of the Mechanical Behavior of Biomedical Materials*, 50, 277-289.
20. Mkhabela, V.; and Ray, S.S. (2015). Biodegradation and bioresorption of poly(ε-caprolactone) nanocomposite scaffolds. *International Journal of Biological Macromolecules*, 79, 186-192.
21. Li, X.M.; Feng, Q.L.; and Cui, F.Z. (2006). In vitro degradation of porous nano-hydroxyapatite/collagen/PLLA scaffold reinforced by chitin fibres. *Materials Science and Engineering: C*, 26(4), 716-720.

22. Gigli, M.; Fabbri, M.; Lotti, N.; Gamberini, R.; Rimini, B.; and Munari, A. (2016). Poly(butylene succinate)-based polyesters for biomedical applications: A review. *European Polymer Journal*, 75, 431-460.
23. Zou, B.; Li, X.H.; Zhuang, H.H.; Cui, W.G.; Zou, J.; and Chen, J.G. (2011). Degradation behaviors of electrospun fibrous composites of hydroxyapatite and chemically modified poly(DL-lactide). *Polymer Degradation and Stability*, 96(1), 114-122.
24. Kasuga, T.; Ota, Y.; Nogami, M.; and Abe, Y. (2001). Preparation and mechanical properties of polylactic acid composites containing hydroxyapatite fibers. *Biomaterials*, 22(1), 19-23.
25. Liuyun, J.; Chengdong, X.; Lixin, J.; and Lijuan, X. (2014). Effect of hydroxyapatite with different morphology on the crystallization behavior, mechanical property and in vitro degradation of hydroxyapatite/poly(lactic-co-glycolic) composite. *Composites Science and Technology*, 93, 61-67.
26. Petricca, S.E.; Marra, K.G.; and Kumta, P.N. (2006). Chemical synthesis of poly(lactic-co-glycolic acid)/hydroxyapatite composites for orthopaedic applications. *Acta Biomaterialia*, 2(3), 277-286.
27. Eftekhari, S.; Sawi, I.E.; Bagheri, Z.S.; Turcotte, G.; and Bougherara, H. Fabrication and characterization of novel biomimetic PLLA/cellulose/hydroxyapatite nanocomposite for bone repair applications. *Materials Science and Engineering: C*, 39, 120-125.
28. Lee, Y.H.; Lee, J.H.; An, I.G.; Kim, C.; Lee, D.S.; Lee, K.W.; and Nam, J.D. (2014). Electrospun dual-porosity structure and biodegradation morphology of Montmorillonite reinforced PLLA nanocomposite scaffolds. *Biomaterials*, 26(16), 3165-3172.
29. Stloukal, P.; Kalendova, A.; Mattausch, H.; Laske, S.; Holzer, C.; and Koutny, M. (2015). The influence of a hydrolysis-inhibiting additive on the degradation and biodegradation of PLA and its nanocomposites. *Polymer Testing*, 41, 124-132.
30. Rapacz-Kmita, A.; Stodolak-Zych, E.; Szaraniec, B.; Gajek, M.; and Dudek, P. (2015). Effect of clay mineral on the accelerated hydrolytic degradation of polylactide in the polymer/clay nanocomposites. *Material Letters*, 146, 73-76.
31. Jiang, L.; Zhang, J.W.; and Wolcott, M.P. (2007). Comparison of polylactide/nano-sized calcium carbonate and polylactide/montmorillonite composites: Reinforcing effects and toughening mechanisms. *Polymer*, 48(26), 7632-7644.
32. Ruiz-Hitzky, E.; Darder, M.; Fernandes, F.M.; Wicklein, B.; Alcântara, A.C.S.; and Aranda, P. (2013). Fibrous clays based bionanocomposites. *Progress in Polymer Science*, 38(10-11), 1392-1414.
33. Michael, F.M.; Khalid, M.; Walvekar, R.; Ratnam, C.T.; Ramarad, S.; Siddiqui, H.; and Hoque, M.E. (2016). Effect of nanofillers on the physico-mechanical properties of load bearing bone implants. *Materials Science and Engineering: C*, 67, 792-806.
34. Cai, X.; Tong, H.; Shen, X.Y.; Chen, W.X.; Yan, J.; and Hu, J.M. (2009). Preparation and characterization of homogeneous chitosan-polylactic acid/hydroxyapatite nanocomposite for bone tissue engineering and evaluation of its mechanical properties. *Acta Biomaterialia*, 5(7), 2693-2703.

35. Mostafa, A.A.; Oudadesse, H.; Mohamed, M.B.; Foad, E.S.; Gal, Y.L.; and Cathelineau, G. (2009). Convenient approach of nanohydroxyapatite polymeric matrix composites. *Chemical Engineering Journal*, 153(1-3), 187-192.
36. Babaei, Z.; Jahanshahi, M.; and Rabiee, S.M. (2013). The fabrication of nanocomposites via calcium phosphate formation on gelatin-chitosan network and the gelatin influence on the properties of biphasic composites. *Materials Science and Engineering: C*, 33(1), 370-375.
37. Jing, X.; Mi, H.Y.; and Turng, L.S. (2017). Comparison between PCL/hydroxyapatite (HA) and PCL/halloysite nanotube (HNT) composite scaffolds prepared by co-extrusion and gas foaming. *Materials Science and Engineering: C*, 72, 53-61.
38. Basha, R.Y.; Kumar, T.S.S.; and Doble, M. (2015). Design of biocomposite materials for bone tissue regeneration. *Materials Science and Engineering: C*, 57, 452-463.
39. Sunil, B.R.; and Jagannatham, M. (2016). Producing hydroxyapatite from fish bones by heat treatment. *Material Letters*, 185, 411-414.
40. Ferraro, V.; Carvalho, A.P.; Piccirillo, C.; Santos, M.M.; Castro, P.M.L.; and Pintado, M.E. (2013). Extraction of high added value biological compounds from sardine, sardine-type fish and mackerel canning residues - A review. *Materials Science and Engineering: C*, 33(6), 3111-3120.
41. Mohammadi, M.; Ziaie, F.; Majdabadi, A.; Akhavan, A.; and Shafaei, M. (2017). Improvement of mechanical and thermal properties of high energy electron beam irradiated HDPE/hydroxyapatite nano-composite. *Radiation Physics and Chemistry*, 130, 229-235.
42. Shayan, M.; Azizi, H.; Ghasemi, I.; and Karrabi, M. (2015). Effect of modified starch and nanoclay particles on biodegradability and mechanical properties of cross-linked poly lactic acid. *Carbohydrate Polymers*, 124, 237-344.
43. Zaidi, L.; Bruzaud, S.; Bourmaud, A.; Me´de´ric, P.; Kaci, M.; and Grohens, Y. (2010). Relationship between structure and rheological, mechanical and thermal properties of polylactide/cloisite 30B nanocomposites. *Journal of Applied Polymer Science*, 116(3), 1357-1365.
44. Suljovrujić, E.; Ignjatović, N.; Uskoković, D.; Mitrić, M.; Mitrović, M.; and Tomić, S. (2007). Radiation-induced degradation of hydroxyapatite/poly L-lactide composite biomaterial. *Radiation Physics and Chemistry*, 76(4), 722-728.
45. Chen, D.Z.; Tang, C.Y.; Chan, K.C.; Tsui, C.P.; Yu, P.H.F.; Leung, M.C.P.; and Uskokovic, P.S. (2007). Dynamic mechanical properties and in vitro bioactivity of PHBHV/HA nanocomposite. *Composites Science and Technology*, 67(7-8), 1617-1626.
46. Sheikh, Z.S.; Najeeb, S.; Khurshid, Z.; Verma, V.; Rashid, H.; and Glogauer, M. (2015). Biodegradable materials for bone repair and tissue engineering applications. *Materials*, 8(9), 5744-5794.
47. Berger, S.; Müller, E.; and Schnabelrauch, M. (2009). Influence of methacrylate-containing surface modifiers on the mechanical properties of nano-hydroxyapatite/polylactide network composites. *Material Letters*, 63(30), 2714-2717.

48. Davachi, S.M.; Heidari, B.S.; Hejazi, I.; Seyfi, J.; Oliaei, E.; Farzaneh, A.; and Rashedi, H. (2017). Interface modified polylactic acid/starch/poly ε-caprolactone antibacterial nanocomposite blends for medical applications. *Carbohydrate Polymers*, 155, 336-344.
49. Markoˇciˇc, E.; Skerget, M.; and ˇKnez, Z. (2011). Solubility and diffusivity of CO_2 in poly(L-lactide)-hydroxyapatite and poly(D,L-lactide-co-glycolide)-hydroxyapatite composite biomaterials. *Journal of Supercritical Fluids*, 55(3), 1046-1051.
50. Neuendorf, R.E.; Saiz, E.; Tomsia, A.P.; and Ritchie, R.O. (2008). Adhesion between biodegradable polymers and hydroxyapatite: Relevance to synthetic bone-like materials and tissue engineering scaffolds. *Acta Biomaterialia*, 4(5), 1288-1296.
51. Chen, L.J.; and Wang, M. (2002). Production and evaluation of biodegradable composites based on PHB-PHV copolymer. *Biomaterials*, 23(13), 2631-2639.
52. Neto, W.A.R.; Pereira, I.H.L.; Ayres, E.; de-Paula, A.C.C.; Averous, L.; Góes, A.M.; Oréfice, R.L.; Bretas, R.E.S. (2012). Influence of the microstructure and mechanical strength of nanofibers of biodegradable polymers with hydroxyapatite in stem cells growth. Electrospinning, characterization and cell viability. *Polymer Degradation and Stability*, 97(10), 2037-2051.
53. Bhowmik, R.; Katti, K.S.; and Katti, D. (2007). Molecular dynamics simulation of hydroxyapatiteepolyacrylic acid interfaces. *Polymer*, 48(2), 664-674.
54. Depan, D.; Kumar, A.P.; and Singh, R.P. (2009). Cell proliferation and controlled drug release studies of nanohybrids based on chitosan-g-lactic acid and montmorillonite. *Acta Biomaterialia*, 5(1), 93-100.
55. Payne, S.A.; Katti, D.R.; Katti, K.S. (2016). Probing electronic structure of biomineralized hydroxyapatite inside nanoclay galleries. *Micron*, 90, 78-86.